

Image-Based Analysis of Evaporating Diesel Sprays in the Near-Nozzle Region

C. Crua¹, G. de Sercey¹, M. Gold², M. R. Heikal¹

1: Centre for Automotive Engineering, University of Brighton, UK

2: BP Formulated Products Technology, Pangbourne, UK

Abstract

Detailed measurements of near-nozzle spray formation is essential to better understand and predict the processes involved in diesel fuel atomisation. We previously showed that direct imaging with sub-micron resolution could yield droplet size measurements in the near-nozzle region under non-evaporative conditions, without an arbitrary requirement for droplet sphericity. We now report on progress made with ongoing experimental investigations at elevated pressure and temperature conditions. We conducted tests on a reciprocating rapid compression machine to produce high-resolution panoramas of the liquid spray interface, compared them with high-speed video frames, and measured droplet sizes at key locations. We also studied the size and shape of liquid structures formed during the end of injection, which were found to be significantly larger and slower than those recorded during injection.

Introduction

Microscopic imaging experiments of diesel sprays have been reported in the literature (e.g. [1-6]), although with varying degrees in the quality of the images produced. Due to recent technological developments, microscopic imaging is now able to provide new information on the liquid and gaseous structures in the near-nozzle region of diesel sprays at elevated pressure and temperature conditions [7-9]. We recently showed that shadowgraphic micrographs could yield droplet size measurements in the near-nozzle region under non-evaporative conditions [10], without an arbitrary requirement for droplet sphericity, but challenges remain to apply this diagnostic to droplet sizing in high pressure and temperature environments. Potential sources of image degradation include motion blurring of fast-moving droplets, the relative motion between the optical chamber and the microscope, as well as the presence of density gradients within the in-cylinder gas, which will result in refractive index fluctuations. Such refractive index gradients have a detrimental effect on both the quality of the back-illumination, and the capability of the optical system to form a focused image of the liquid spray. At the same time, the droplet/gas interface is expected to become distinctly less clear as the droplets evaporate and approach supercritical conditions. Hence, whilst direct imaging has potential for resolving both spherical and arbitrary-shaped droplets in the near-nozzle region of diesel sprays, challenges remain to accurately measure microscopic droplets at evaporating conditions. In this publication we report on progress made with ongoing experimental investigations of the atomisation of diesel fuel at elevated pressure and temperature conditions. We conducted tests on a reciprocating rapid compression machine using high-resolution microscopic imaging and macroscopic high-speed video. We used microscopy to track the periphery of the dense spray and build a panoramic view of the spray interface from the nozzle orifice to 27 mm. We compared the liquid structures with the high-speed video, and measured droplet sizes and velocities at key locations. We then studied the end of injection, and report on the size, velocity and shape of liquid structures observed at the orifice outlet.

Experimental test-rig

The experiment was conducted on a reciprocating rapid compression machine (RCM) based around a Ricardo Proteus single cylinder engine converted to liner ported, 2 stroke cycle operation. The fuel was delivered by a Delphi common-rail system, comprising a DFP-3 high-pressure pump rated at 200 MPa, and a seven-hole DFI-1.3 injector with a VCO type nozzle. The nozzle's orifices were cylindrical with a diameter of 135 μm and a length/diameter ratio of 8. The nozzle had an equivalent cone angle of 154°, and the injector was mounted orthogonal relative to the cameras. The duration of the injection trigger pulse was constant at 700 μs . A detailed description of the test rig is covered by Crua [11].

The fuel used for all results presented in this paper was an ultra-low sulphur fossil diesel fuel, which contained no bio components. Its physical properties are listed in Table 1.

Table 1. Physical properties of the fuel tested

Property	Diesel
Density at 15°C (kg.m ⁻³)	837
Kinematic viscosity (mm ² .s ⁻¹)	3.3
Surface tension (dyn.cm ⁻¹)	29.8

The optical setup was covered in detail by the authors in [7], hence only the main features are included here. The light source was a frequency-doubled Nd:YAG laser, with a pulse duration of 7 ns. The light pulse was spectrally diffused and spatially expanded from 8 mm to 100 mm to provide homogeneous illumination over a sufficiently large area. A high performance dual-frame camera with a Peltier-cooled 12 bit CCD sensor was fitted with a long range microscope. The optical setup was adjusted to optimise both the spatial resolution and the viewing region. This was achieved with a magnification factor of 9.6 at the CCD sensor plane, giving a spatial scale factor of 0.671 μm per pixel and a viewing region of 923x697 μm . The spatial resolution of the optical system was then measured as 1.27 μm for a 3% contrast level. The main experimental conditions for the images presented in this paper are listed in Table 2. The use of a double-pulsed light source combined with a dual-frame camera and an interframe time of 500 ns allowed capturing the velocity of the fuel, as well as the droplet size distribution.

Table 2. Experimental conditions for the microscopic imaging experiments. Timings are relative to start of injection (SOI) trigger.

Injection pressures	40 MPa
Nozzle orifice diameter	135 μm
Gas pressure	3.2 MPa
Gas temperature	700 K
Axial distance from nozzle	0 to 27 mm
Radial distance from axis	0 to 2 mm
Acquisition timing	1 ms after SOI
Image size	1376x1040 pixels
Field of view	923x697 μm
Spatial scale factor	0.671 $\mu\text{m}/\text{pixel}$
Spatial resolution (3% contrast)	1.27 μm

In order to obtain information on the overall structure of the sprays, a Phantom v12.1 high speed camera was used to record the macroscopic evolution of the complete spray. The camera was operated at 41,667 fps with a frame resolution of 256x512 pixels and a spatial scale factor of 83 μm per pixel. In order to avoid motion blur, a copper vapour laser with a 25 ns pulse duration was used to illuminate the sprays at the same frequency as the high-speed camera. The optical setups for microscopy and high-speed video are shown in Figure 1.

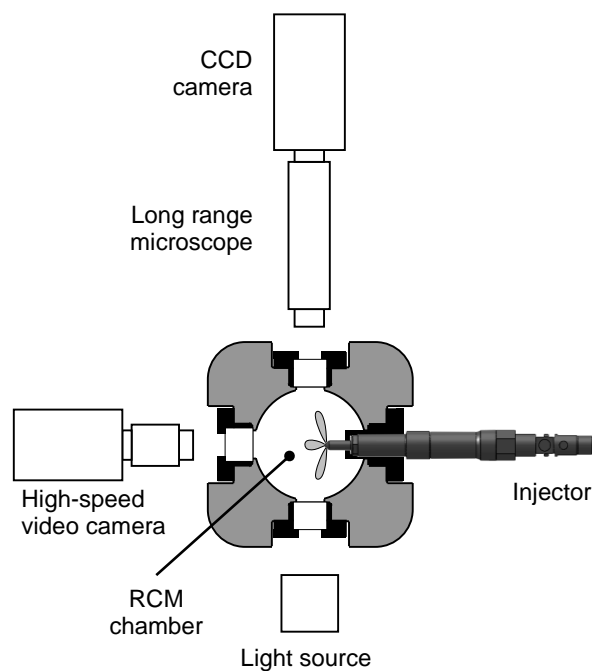


Figure 1. Optical setup for microscopic imaging and macroscopic high-speed video. For the high-speed video experiment the light source was a copper vapour laser pulsing at a frequency of 41,667 Hz.

Results and Discussion

Spray interface

Figure 3 shows a comparison of the shadowgraphs with a high speed video frame taken at the same timing of 1 ms after the start of injection. At this timing the spray is well developed and the fuel delivery rate is steady. Figure 2 shows the mean penetration versus time for a set of 101 individual videos. Figure 3a consists of a panorama of 54 full resolution shadowgraphs tracking the spray interface. Since the maximum repetition rate of the CCD camera is 8 Hz, the images composing this panorama are taken from different sprays. The images marked a1, a2, a3 and a4 are magnified images from the panorama, at position 1, 2, 3 and 4 respectively. Figure 3b shows a high speed video frame from a different cycle, with the position of the panorama outlined. Whilst the video frame captures the overall structure of a single spray, microscopic details are inevitably beyond the spatial resolution of the instrument. In contrast, long-range microscopy can give detailed information about a portion of the spray but at the expense of an understanding of what lies beyond that small region.

Shadowgraphy is sensitive to density gradients, which can be caused by temperature gradients in the gas phase or changes in fuel concentration in the air-fuel mixture. This sensitivity to gas temperature gradients contributes to the distortion of the optical path and often results in defocused shadowgraphs [10]. However, when the images are in focus, this sensitivity allows the capture of the air-fuel mixing (Figure 3a3). It is also possible to observe trails in the wake of some droplets (Figure 3a4; Figure 4), although it is not possible to establish whether they are caused by fuel vapour gradients or temperature gradients.

Near the nozzle (Figure 3a1, 900 μm from the nozzle) and up to 10 mm away, the spray is optically dense with a well-defined interface between ambient gas and liquid spray. Droplets can be seen on the periphery of the dense region, with diameters of the order of 3 μm . Cycle-to-cycle variations in the general appearance of this near-nozzle region are relatively small.

For the first 10 mm of the spray the liquid interface has a markedly conical shape with few signs of vaporised fuel. The boundary of the liquid spray can be tracked without difficulty as it is contained within the width of one or two frames. Beyond 10 mm from the orifice the liquid interface becomes progressively more difficult to identify as cycle-to-cycle variations become larger than the width of a frame. This is expected to be due to small scale recirculation zones caused by air entrainment. Density gradients in the gas phase start to appear, in agreement with the expectation that entrainment of hot gas into the spray promotes evaporation.

Beyond 20 mm from the orifice, the spray becomes dispersed as large clusters of droplets detach ahead of the main liquid jet. Strong density gradients are visible in the gas phase (Figure 3a3; Figure 3a4) most likely due to turbulent mixing of vaporised fuel. As a result the cycle-to-cycle variation of the number density of droplets is significant, with some images containing no liquid drops and others showing dispersed droplets. The droplets contained in these detached clusters can have relatively large diameters and less spherical shapes (Figure 4) than droplets found at the periphery of the near-nozzle region (e.g. Figure 3a1,a2). These clusters are composed of droplets with velocities of 30-40 m/s and diameters up to 20 μm (Figure 4), which could be an indication of droplet coalescence and low relative velocities within the dense spray region.

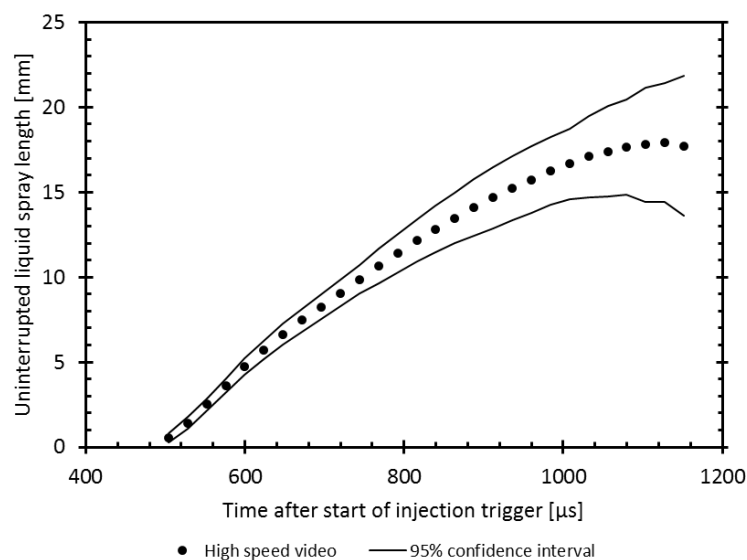


Figure 2. Uninterrupted liquid spray length versus time (mean of 101 videos) and 95% confidence interval (± 2 standard deviations of the set).

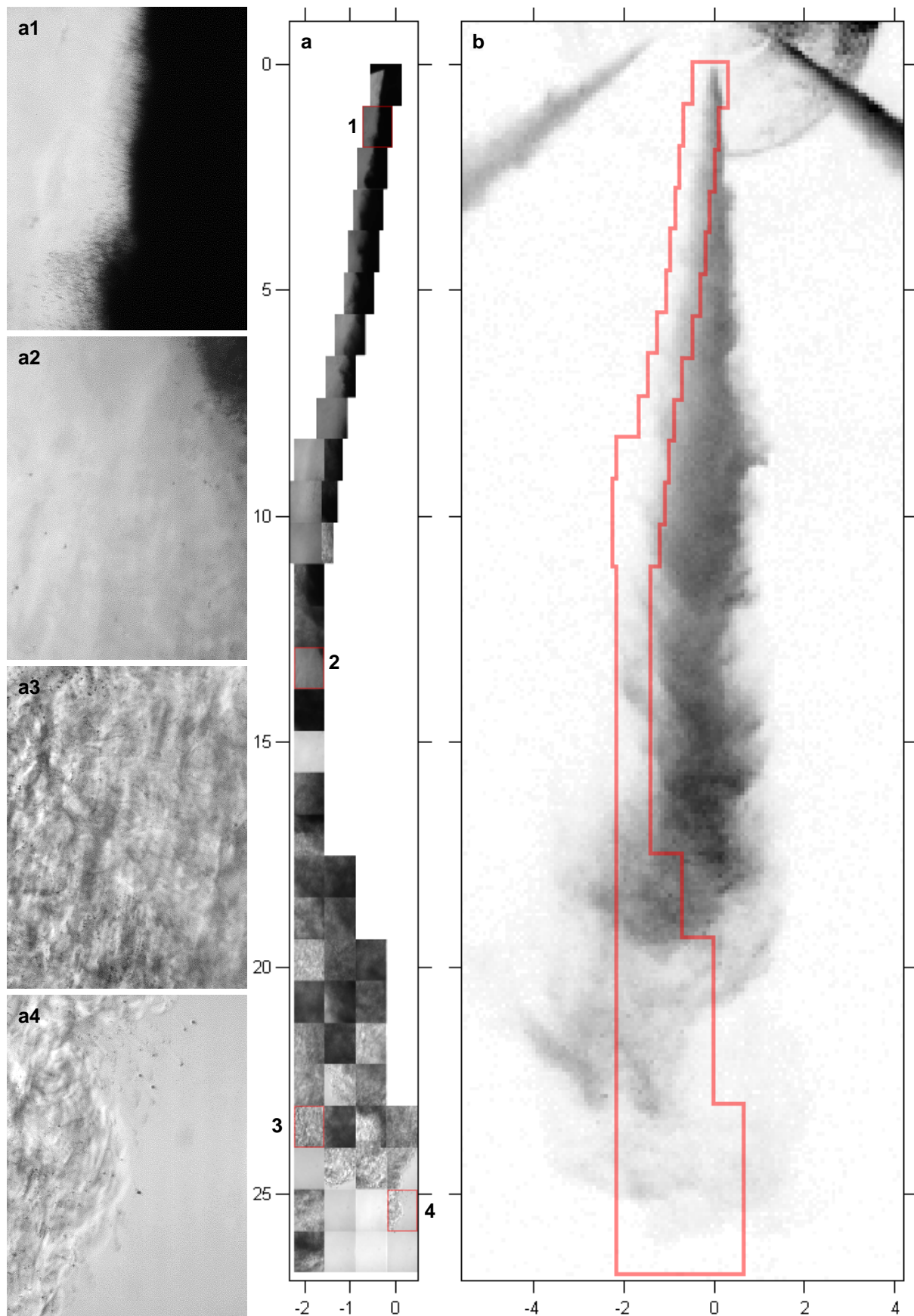


Figure 3. (a) Panorama composed of 54 microscopic shadowgraphs tracking the spray interface. (b) Frame from a high-speed video (intensities inverted for clarity) recorded 1ms after SOI. Scales are in mm from nozzle exit.

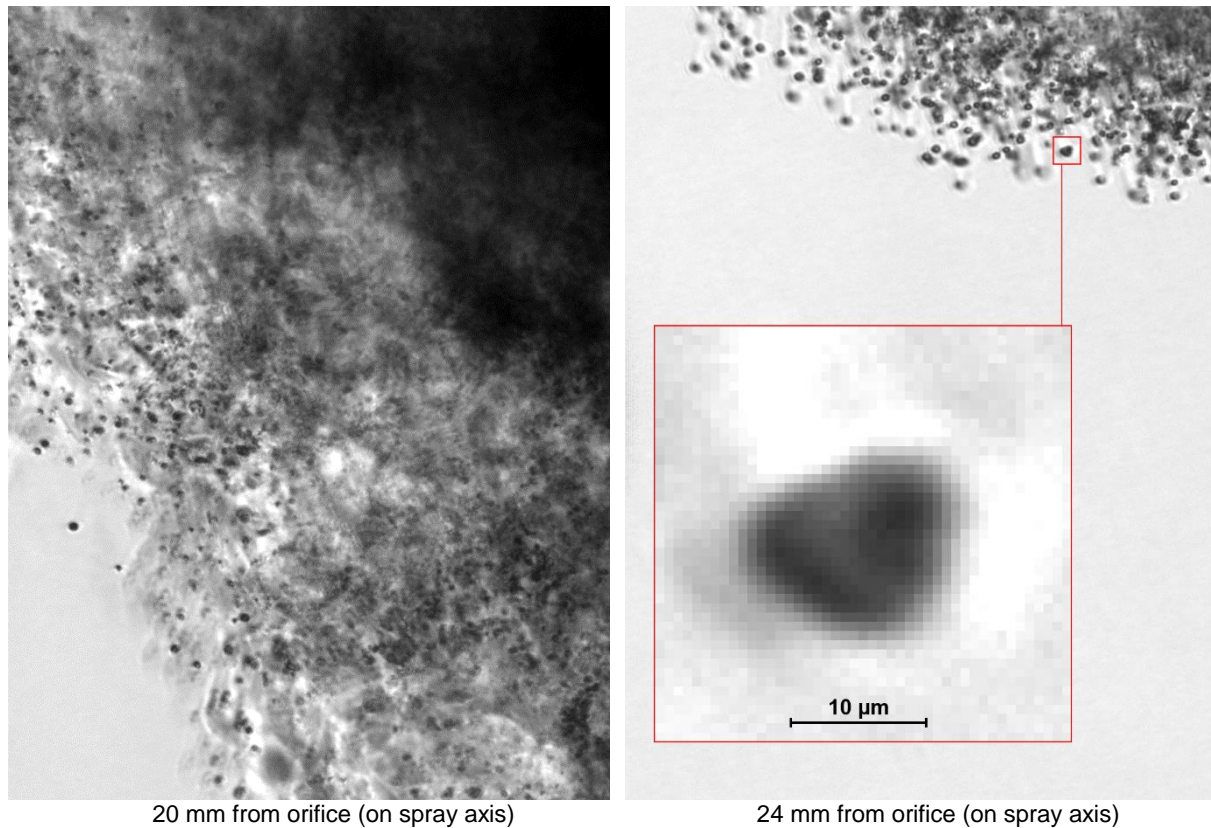


Figure 4. Examples of shadowgraphic micrographs recorded for non-additised fossil diesel fuel injected at 40 MPa into gas at 3.2 MPa pressure and 700 K bulk temperature.

End of injection

In order to characterise the end of injection we recorded shadowgraphs at the nozzle exit from 1 ms to 2.15 ms after the start of injection trigger, with 50 μ s time steps and 50 images recorded per time step. Due to the highly transient nature of the end of injection, it is particularly difficult to define quantitative criteria that can be used to support an objective description of the processes involved. Hence we conduct a descriptive analysis of the series of images captured over the end of injection phase.

As previously discussed, at 1 ms (Figure 5a) the spray is optically dense with little cycle-to-cycle variations in the position of the liquid interface. The droplets that are located at the periphery of the liquid jet have diameters smaller than 5 μ m and velocities between 15 and 30 m/s. As the nozzle closes (Figure 5b) the width of the spray increases in the near-nozzle region and droplet velocities drop to less than 10 m/s. As the fuel mass flow reduces, the spray seems to turn into a liquid sheet structure originating from the nozzle (Figure 5d,e). Within a short distance the sheet appears to break into ligaments with diameters between 10 and 25 μ m. Some dense regions larger than 100 μ m are also present along the spray axis, although it is not clear whether these contain ligaments, droplets or both. The ligaments that are clearly identifiable are surrounded by droplets with equivalent diameters up to 25 μ m. The velocities of liquid structures shown in Figure 5d,e are below 10 m/s, with many being below the lower limit of our system (2.6 m/s). At this transient stage the cycle-to-cycle variation naturally increases but the majority of images appear similar to Figure 5d with some resembling Figure 5f. At 1.5 ms after SOI large deformed ligaments appear (Figure 5f) with widths of 20 to 50 μ m and length of more than 600 μ m. In agreement with other studies [9], these liquid structures are much larger than those found during the steady state part of injection. The ligament in that figure appears to be undergoing breakup into relatively large droplets. Again, velocities are low, suggesting that some of these droplets may re-coalesce into larger ones. This could contribute to the formation of large droplets that were observed 2 ms after the start of injection (Figure 5h), some big droplets are sometimes visible. The presence of such large liquid structures when combustion would normally occur may have an effect on emissions, and warrants further investigations into the processes involved.

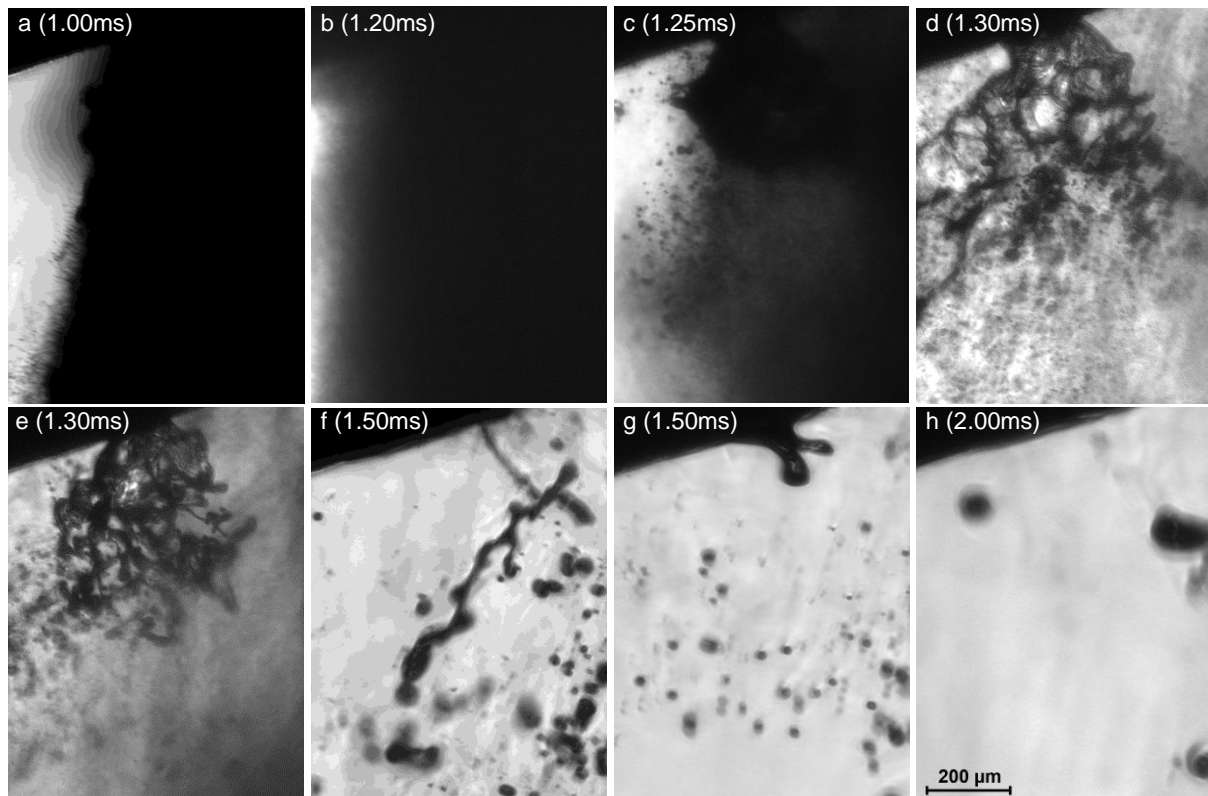


Figure 5. Evolution of the end of injection, timings relative to SOI trigger.

Conclusions

We conducted tests on a reciprocating rapid compression machine using high-resolution microscopic imaging and macroscopic high-speed video. We used microscopy to track the periphery of the dense spray and build a panoramic view of the spray interface from the nozzle orifice to 27 mm. We compared the liquid structures with the high-speed video, and measured droplet sizes and velocities at key locations.

Beyond 20 mm from the orifice, the spray was relatively dispersed as large clusters of droplets detach ahead of the main liquid jet. Strong density gradients were visible in the gas phase, most likely due to turbulent mixing of vaporised fuel. The droplets contained in these detached clusters were found to have diameters up to 20 μm , velocities in the region of 30-40 m/s, and some droplets had non-spherical shapes. These could be an indication of droplet coalescence and low relative velocities within the dense spray region.

We studied the end of injection and observed significantly larger and slower liquid structures than those recorded during injection. The volume of liquid contained in these large deformed structures, at a time when combustion would normally occur, could have a non-negligible effect on emissions which warrants further investigations into the processes involved.

Acknowledgements

This work received financial and technical supported from BP International Ltd; and financial support from the European Regional Development Fund [INTERREG IVa project ‘E3C3’, grant number 4274].

References

1. Heimgärtner, C. and A. Leipertz, *Investigation of Primary Diesel Spray Breakup Close to the Nozzle of a Common Rail High Pressure Injection System*, in *8th ICLASS*. 2000: Pasadena, USA. p. 1235-1241.
2. Bae, C., et al., *Effect on nozzle geometry on the common-rail diesel spray*. SAE 2002-01-1625, 2002.
3. Badock, C., et al., *Investigation of Cavitation in Real Size Diesel Injection Nozzles*. International Journal of Heat and Fluid Flow, 1999. **20**(5): p. 538-544.
4. Lai, M., et al., *Microscopic Characterization of Diesel Sprays at VCO Nozzle Exit*. SAE transactions, 1998. **107**: p. 1283-1293.
5. Sjöberg, H., G. Manneberg, and A. Cronhjort, *Long-working-distance microscope used for diesel injection spray imaging*. Optical Engineering, 1996. **35**: p. 3591.

6. Badock, C., et al., *Investigation of Cavitation in Real Size Diesel Injection Nozzles*. International Journal of Heat and Fluid Flow 20(5), 1999: p. 538-544.
7. Crua, C., et al., *High-Speed Microscopic Imaging of the Initial Stage of Diesel Spray Formation and Primary Breakup*, in *SAE paper 2010-01-2247*. 2010.
8. Shoba, T., et al., *Optical Characterisation of Diesel, RME and Kerosene Sprays by Microscopic Imaging*, in *24th ILASS-Europe*. 2011: Estoril, Portugal.
9. Manin, J., A. Kastengren, and R. Payri *Understanding the acoustic oscillations observed in the injection rate of a common-rail direct injection diesel injector*. Journal of Engineering for Gas Turbines and Power, 2012. DOI: 10.1115/1.4007276.
10. Crua, C., G. de Sercey, and M.R. Heikal, *Dropletsizing of Near-Nozzle Diesel and RME Sprays by Microscopic Imaging*, in *12th ICLASS*. 2012: Heidelberg, Germany.
11. Crua, C., *Combustion Processes in a Diesel Engine*, in *School of Engineering*. 2002, University of Brighton: Brighton.